Network: Computation in Neural Systems
June 2006; 17: 131–150

Taylor & Francis
Taylor & Francis Group

Mean field theory for a balanced hypercolumn model of orientation selectivity in primary visual cortex

ALEXANDER LERCHNER,[1] GUSTAF STERNER,[2] JOHN HERTZ,[3] & MANDANA AHMADI[3]

[1] *Technical University of Denmark, 2800 Lyngby, Denmark,* [2] *Department of Physics, University of Rochester, Rochester, NY, USA and* [3] *Nordita, Blegdamsvej 17, 2100 Copenhagen Ø, Denmark*

(Received 25 March 2004; revised 16 May 2005; accepted 31 October 2005)

Abstract
We present a complete mean field theory for a balanced state of a simple model of an orientation hypercolumn, with a numerical procedure for solving the mean-field equations quantitatively. With our treatment, one can determine self-consistently both the firing rates and the firing correlations, without being restricted to specific neuron models. Here, we solve the mean-field equations numerically for integrate-and-fire neurons. Several known key properties of orientation selective cortical neurons emerge naturally from the description: Irregular firing with statistics close to – but not restricted to – Poisson statistics; an almost linear gain function (firing frequency as a function of stimulus contrast) of the neurons within the network; and a contrast-invariant tuning width of the neuronal firing. We find that the irregularity in firing depends sensitively on synaptic strengths. If the Fano factor is considerably larger (smaller) than 1 at some stimulus orientation, then it is also larger (resp. maller) than 1 for all other stimulus orientations that elicit firing. We also find that the tuning of the noise in the input current is the same as the tuning of the external input, while that for the mean input current depends on both the external input and the intracortical connectivity.

Keywords: *Mean-field theory, primary visual cortex, Fano factor, orientation tuning, contrast invariance*

Introduction

Neurons in primary visual cortex (V1) fire highly irregularly in response to visual stimuli, but with reproducible firing rates. They do so despite the fact that they receive synaptic input from thousands of other cortical neurons, which would lead to fluctuations in the input that were small compared to the mean if excitatory and inhibitory inputs were not balanced (Softky & Koch 1993). There has been some success in describing how such a balance can emerge self-consistently from dynamics that are plausible for cortical networks. This was accomplished by mean field-descriptions by van Vreeswijk and Sompolinsky, (1996, 1998), Amit and Brunel (1997a, b) and Brunel (2000). However, their treatments do not permit a self-consistent calculation of firing correlations. How to do this correctly was first shown for an all-inhibitory network by Hertz et al. (2003) using the systematic formulation of mean field theory due to Fulvi Mari (2000). In a recent paper (Lerchner et al. 2006) we presented a mean-field theory

Correspondence: Alexander Lerchner, Laboratory of Neuropsychology Bldg. 49 Rm. 1B80, National Institutes of Health, 49 Convent Dr., Bethesda, MD 20892, USA. Tel: 301-694-5625 ext. 254; Fax: 301-402-0046; E-mail: LerchnerA@mail.nih.gov

ISSN: 0954-898X print / ISSN 1361-6536 online
DOI: 10.1080/09548980500444933

for a balanced network model that allowed us to quantify how the irregularity in firing and, more generally, the firing correlations depend on intrinsic network properties such as synaptic strengths. The analysis was applied to a statistically homogeneous network, representing a cortical column composed of neurons with similar response characteristics. Here, we show how to extend this treatment to networks with systematic structure, consisting of multiple cortical columns. In particular, we model an orientation hypercolumn, composed of a set of orientation columns.

An orientation column contains neurons that respond strongest to elongated visual stimuli of a specific orientation, the *preferred orientation* (PO). Orientation selective neurons exhibit a tuned response to other orientations, with sharply decreasing firing rates as the similarity between PO and stimulus orientation decreases, until the firing is completely suppressed for orientations outside the *tuning width* of the neuron in question. An important feature of orientation tuning is that the tuning width is independent of the stimulus contrast (Sclar & Freeman 1982). It is not possible to capture this feature in a single-neuron description using a Hubel and Wiesel feed-forward connectivity (Hubel & Wiesel 1962) from the lateral geniculate nucleus (LGN); rather, cortical interactions are needed to achieve contrast-invariant tuning (for review see Sompolinsky & Shapley 1997). Ben-Yishai et al. (1995) proposed a model for which the tuning width is independent of the contrast, but a threshold-linear relationship between input current and firing rate was an assumption of the model, and the problem of the firing statistics was not addressed.

Here, we show how a contrast-invariant tuning width, an almost linear input–output relationship, and irregular firing can all be explained by a balanced hypercolumn model. With our mean-field treatment, we can quantify how certain network properties like synaptic strengths, tuning of the LGN input and of the intracortical connectivity influence the statistics and tuning of the neuronal firing. Using the Fano factor F (the ratio of spike count variance and mean spike count) to quantify the irregularity in firing, we find, e.g., that if F is significantly greater than 1 the orientation tuning of F reaches a maximum at the PO. Fano factors greater than 1 are normally observed for neurons in V1 (see, e.g., Gershon et al. 1998). We also make quantitative predictions about the tuning of the input currents and their fluctuations.

The model

We model a single orientation hypercolumn in primary visual cortex, with a simplified network architecture as indicated in Figure 1. The network comprises an excitatory population and an inhibitory one, of sizes N_1 and N_2, respectively. Each population is divided into n subpopulations (orientation columns), parameterized by an angle θ. The angles, spaced equally between $-\pi/2$ and $\pi/2$, indicate the preferred orientation (PO), to which the neurons in the corresponding column respond strongest.

We use leaky integrate-and-fire neurons and interconnect them randomly with a connection probability $P_{ab}(\theta - \theta')$ that depends on the similarity of the POs. The probability that a neuron with PO θ (in population a) receives afferent input from a neuron with PO θ' in population b is taken as

$$P_{ab}(\theta - \theta') = \frac{K_b}{N_b}(1 + \gamma \cos 2(\theta - \theta')), \tag{1}$$

where K_b is the expected overall number of inputs from neurons in population b. We take the ratio K_b/N_b independent of $b \in \{1, 2\}$, i.e., excitatory and inhibitory neurons interconnect with the same probability in our model. The functional form of Equation 1 is motivated by anatomical evidence that the connection probability between cortical neurons decreases as

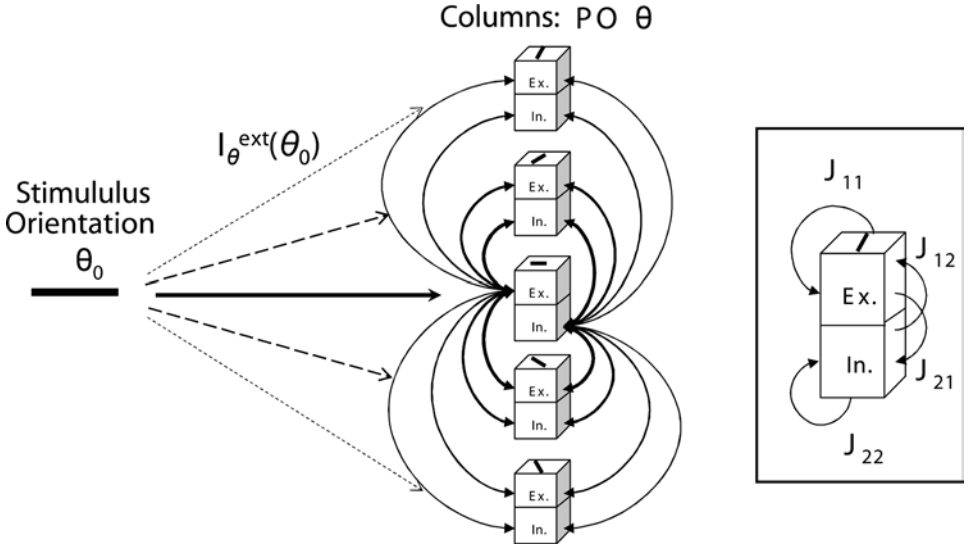

Figure 1. Structure of the model network. The hypercolumn consists of multiple orientation columns, each of which has an excitatory and an inhibitory subpopulation and is assigned a preferred orientation (PO) θ. Columns with more similar POs share on average more connections than more dissimilar ones (the density of connections is indicated only between one column and the rest, for clarity). The network receives excitatory external input, weakly tuned to the stimulus orientation θ_0. The inset shows a sketch for the connectivity and connection strengths $\mathcal{J}_{ab}$ within an orientation column.

their distance increases, and by the fact that orientation columns with similar PO tend to lie closer together on the cortical surface than ones with dissimilar PO. We followed Ben-Yishai et al. (1995) in choosing the simplest possible form that is periodic with period π. We assume that the degree of tuning, as measured by the parameter $\gamma \in (0, 1)$, is the same for both the inhibitory and the excitatory population.

Each nonzero synapse from a neuron in population b to one in population a is taken to have strength

$$\mathcal{J}_{ij}^{a\theta,b\theta'} = \frac{\mathcal{J}_{ab}}{\sqrt{K_b}} \tag{2}$$

where the parameters $\mathcal{J}_{ab}$ are of order 1. With this scaling, the fluctuations in the input current are also of order 1, the same order as the distance between reset and threshold of our model neurons (cf. van Vreeswijk & Sompolinsky 1996, 1998).

The subthreshold dynamics of the membrane potentials are given by

$$\frac{\mathrm{d}u_i^{a\theta}(t)}{\mathrm{d}t} = -\frac{u_i^{a\theta}(t)}{\tau} + I_{a\theta}^{\mathrm{ext}}(\theta_0) + I_i^{a\theta,\mathrm{rec}}(t), \tag{3}$$

where the membrane time constant τ is chosen to be the same for all neurons. The excitatory external input from the LGN, $I_{a\theta}^{\mathrm{ext}}(\theta_0)$, is assumed to be (weakly) tuned to the orientation θ_0 of the stimulus due to a feed-forward connectivity from the LGN as in the classical model by Hubel and Wiesel (1962). For simplicity, we take it to be constant in time and the same for all neurons i within a column. The functional form we use is, similar to the tuning (Equation 1) of the intracortical connectivity,

$$I_{a\theta}^{\mathrm{ext}}(\theta_0) = I_a^{\mathrm{ext}}(1 + \epsilon \cos 2(\theta - \theta_0)), \tag{4}$$

where $\epsilon \in (0, 1)$ is the degree of tuning, which is assumed to be the same for both populations. (The condition $\epsilon < 1$ assures $I_{a\theta}^{\mathrm{ext}}(\theta_0)$ to be non-negative, i.e., excitatory, for all orientations). A more detailed model for this external input current, including temporal fluctuations and random connectivity, was briefly described in an overview article by Hertz et al. (2004).

The recurrent input $I_i^{a\theta,\mathrm{rec}}(t)$ from within the model cortex is given by

$$I_i^{a\theta,\mathrm{rec}}(t) = \sum_{b=1}^{2} \sum_{\theta'=\theta_1}^{\theta_n} \sum_{j=1}^{N_b/n} \mathcal{J}_{ij}^{a\theta,b\theta'} S_j^{b\theta'}(t), \tag{5}$$

where $S_j^{b\theta'}(t) = \sum_s \delta(t - t_{j\theta' b}^s)$ is the spike train of neuron j with PO θ' in population b.

Mean field theory

In the following mean-field analysis of the orientation hypercolumn model, we consider stationary firing only, for simplicity. However, the formulation is general enough to allow for non-stationary rates. We presented such a time-dependent treatment for a balanced single-column model elsewhere (Lerchner et al. 2006).

Mean-field description

We analyze the model for the case of large but extremely dilute connectivity (i.e., $K_b \gg 1$, but $K_b/N_b \to 0$), so that each neuron receives a high number of uncorrelated inputs. According to the central limit theorem, the recurrent input currents given by Equation 5 can therefore be described as Gaussian random processes. For stationary rates, the mean input current is constant in time for any given neuron, although the level of the mean does vary from neuron to neuron due to the random connectivity. In a general mean-field theory, one must consider temporal correlations in these currents, i.e., not restrict the description of the random processes to white noise.

To separate the mean of the currents from their fluctuations ('noise'), it is convenient to apply such separations to the description of both the synaptic weights $\mathcal{J}_{ij}^{a\theta,b\theta'}$ and the spike trains $S_j^{b\theta'}(t)$ in Equation 5. For the weights we can write

$$\mathcal{J}_{ij}^{a\theta,b\theta'} = \overline{\mathcal{J}_{ij}^{a\theta,b\theta'}} + \delta\mathcal{J}_{ij}^{a\theta,b\theta'}, \tag{6}$$

where the bar means averaging over the index j, i.e., the neurons in the source population:

$$\overline{\mathcal{J}_{ij}^{a\theta,b\theta'}} = \frac{1}{N_b/n} \sum_{j=1}^{N_b/n} \mathcal{J}_{ij}^{a\theta,b\theta'}. \tag{7}$$

Generally, we use the bar-notation for averaging over neuron populations, which will always apply to the running index j in this work. To separate the spike trains into static and dynamic components, we write

$$S_j^{b\theta'}(t) = r_{b\theta'} + \delta r_j^{b\theta'} + \delta S_j^{b\theta'}(t), \tag{8}$$

where $r_{b\theta'} = \overline{r_j^{b\theta'}} = 1/(N_b/n) \sum_j r_j^{b\theta'}$ is the average rate of the neurons in sub-population θ' of population b. The difference between this average rate and the actual rate of neuron j is denoted $\delta r_j^{b\theta'}$. These two components are both static, describing time-averaged quantities. The temporal fluctuations of the spike train and their possible correlations in time are captured by the third term on the right-hand side of Equation 8, $\delta S_j^{b\theta'}(t)$. Using the central

limit theorem and methods like those in Fulvi Mari (2000) and Kree and Zippelius (1987) we can then derive the following mean-field formulation of the recurrent current:

$$I_{a\theta}^{\mathrm{rec}}(t) = \sum_{b=1}^{2} \mathcal{J}_{ab}(\sqrt{K_b}A_b + B_b(t)), \tag{9}$$

with

$$A_b = \frac{1}{n}\sum_{\theta'=\theta_1}^{\theta_n}(1+\gamma\cos 2(\theta-\theta'))r_{b\theta'} \tag{10}$$

$$B_b(t) = \frac{1}{n}\sum_{\theta'=\theta_1}^{\theta_n}\sqrt{1+\gamma\cos 2(\theta-\theta')}\left(\left(\overline{\left(r_j^{b\theta'}\right)^2}\right)^{\frac{1}{2}}x_{b\theta'} + \xi_{b\theta'}(t)\right) \tag{11}$$

where the values $x_{b\theta'}$ are drawn from a unit-variance normal distribution. We have dropped the neuron index i because this statistical description of the input current reduces the network problem to single neuron problems – one for each column population, indexed by $a\theta$. The terms $\xi_{b\theta'}(t)$ stand for realizations of Gaussian random processes obeying

$$\langle \xi_{b\theta'}(t)\xi_{b\theta'}(t')\rangle = C_{b\theta'}(t-t'). \tag{12}$$

Here, $C_{b\theta'}(t-t')$ denotes the average autocorrelation function of the fluctuations in the spike trains of neurons with PO θ' in population b, given by

$$C_{b\theta'}(t-t') = \frac{1}{N_b/n}\sum_{j=1}^{N_b/n}\langle \delta S_j^{b\theta'}(t)\delta S_j^{b\theta'}(t')\rangle. \tag{13}$$

With the operation $\langle\cdot\rangle$ we mean averaging over realizations of random processes, such as stochastic spike trains. We will refer to such realizations as 'trials' since they represent (responses to) repeated presentations of the same stimulus in experimental settings.

Analytical treatment

In general, it is not possible to solve the mean-field equations (9–11) for the neuronal input current analytically. We can, however, derive approximate solutions for the average firing rate for each orientation column, and thus for the average orientation tuning of neurons in the network. On one hand, this will provide us with qualitative insight into fundamental properties of the network, such as an approximate linear dependence of the firing rate on the stimulus contrast, and an on-average contrast-invariant tuning width. On the other hand, this will also provide us with a starting point for the iterative numerical procedure described in the following section that will allow us to solve the mean-field equations for specific parameter values.

Population firing rates. The input currents from the excitatory population and the inhibitory population have mean values of order $\sqrt{K_1} \gg 1$ and $\sqrt{K_2} \gg 1$, respectively (see Equation 9). In addition, for the external input current (Equation 4) we take $I_a^{\mathrm{ext}} = \sqrt{K_0}\hat{I}_a^{\mathrm{ext}}$ with $\sqrt{K_0} \gg 1$. If the neurons are to exhibit irregular firing at a low rate, as cortical neurons do, these currents must nearly cancel and threshold crossings have to be caused by the fluctuations in the currents, which are of order 1. For our orientation hypercolumn model, this 'balance condition' implies that the average input currents in Equation 3 have to nearly cancel for

each orientation column θ:

$$\sqrt{K_0}\hat{I}_a^{\text{ext}}(1+\epsilon\cos 2(\theta-\theta_0))+\sum_{b=1}^{2}\mathcal{J}_{ab}\sqrt{K_b}A_b=\mathcal{O}(1), \tag{14}$$

where A_b is defined in Equation 10. Here, we have ignored the contribution of the leakage current (the first term on the right-hand side of Equation 3), because it is small compared to the input currents, and because the balance condition (Equation 14) holds only up to corrections of $\mathcal{O}(1)$.

To solve these equations, we consider a continuum formulation for the weighted average over all angles instead of the discrete formulation in Equation 10 and write

$$A_b=\int_{-\pi/2}^{\pi/2}\frac{\mathrm{d}\theta'}{\pi}(1+\gamma\cos 2(\theta-\theta'))r_{b\theta'}. \tag{15}$$

Then Equation 14 becomes a pair of integral equations for $r_{a\theta}$. In addition, we will ignore the terms of $\mathcal{O}(1)$ in the balance condition by setting the right-hand side of Equation 14 to zero. This simplification will lead to an approximate solution for the population firing rates that is close to, but not exactly equal to, the correct solution determined later with the numerical procedure.

In the *broadly tuned case* (all orientation columns respond with non-vanishing mean rates to every stimulus orientation), these integral equations can be solved directly. To do so, we perform a Fourier expansion centered at θ_0 of the mean rate within orientation column θ' and write $r_{b\theta'}=r_{b,0}+r_{b,2}\cos 2(\theta'-\theta_0)+\cdots$. For both the input current and the connection probabilities, we have already used such Fourier notations with the fewest possible terms to retain a periodic function with period π. Due to that choice, all higher Fourier components for the mean currents vanish as well, and we get

$$\sqrt{K_0}\hat{I}_a^{\text{ext}}(1+\epsilon\cos 2(\theta-\theta_0))+\sum_{b=1}^{2}\sqrt{K_b}\mathcal{J}_{ab}\left[r_{b,0}+\frac{1}{2}\gamma r_{b,2}\cos 2(\theta-\theta_0)\right]=0. \tag{16}$$

By solving for each of the two Fourier components of the mean rates separately, we obtain

$$r_{a,0}=-\sum_{b=1}^{2}(\hat{\mathrm{J}}^{-1})_{ab}\hat{I}_b^{\text{ext}} \tag{17}$$

$$r_{a,2}=-\frac{2\epsilon}{\gamma}\sum_{b=1}^{2}(\hat{\mathrm{J}}^{-1})_{ab}\hat{I}_b^{\text{ext}}=\frac{2\epsilon}{\gamma}r_{a,0}, \tag{18}$$

where the matrix $\hat{\mathrm{J}}$ is composed of the elements $\hat{\mathcal{J}}_{ab}=\mathcal{J}_{ab}\sqrt{K_b/K_0}$. Firing rates have to be non-negative, so this solution can only be valid for $\epsilon\in(0,\gamma/2]$. However, such a broad tuning is not normally observed for cortical neurons. Rather, orientation sensitive neurons tend to be more 'narrowly tuned', with firing suppressed for stimulus orientations θ_0 that differ too much from the neuron's preferred orientation θ: $r_a=0$ for $|\theta-\theta_0|\geq\theta_c$ for some tuning width θ_c. Within the parameter regime $\epsilon\in(\gamma/2,\gamma]$ we find such narrowly tuned solutions to our model. The tuning width θ_c turns out to be the same for both excitatory and inhibitory neurons, which is a consequence of the population-independence of the tuning parameters ϵ and γ.

To find approximate solutions for the *narrowly tuned case*, we use our insight from the broadly tuned case and make the *ansatz*

$$r_{b\theta'} = \begin{cases} r_{b,0} + r_{b,2}\cos 2(\theta' - \theta_0) & \text{for } |\theta' - \theta_0| < \theta_c^b \\ 0 & \text{for } |\theta' - \theta_0| \geq \theta_c^b, \end{cases} \tag{19}$$

where $\theta_c^b = -1/2\cos^{-1}(r_{b,0}/r_{b,2})$. As mentioned above, since we have assumed equal tuning in (1), θ_c^b is the same for both b. Thus, in Equation 15 the integration is restricted to $|\theta' - \theta_0| < \theta_c$. Because $r_{b\theta'} = 0$ at $\theta' - \theta_0 = \theta_c$, we can rewrite the part of the *ansatz* for $|\theta' - \theta_0| < \theta_c$ in the form

$$r_{b\theta'} = r_{b,2}(\cos 2(\theta' - \theta_0) - \cos 2\theta_c). \tag{20}$$

With this approach, we can indeed find (approximate) solutions for the tuning width and the rates from the balance condition (Equation 14) with the right-hand side set to zero. Analogous to the solution for the broadly tuned case Equation 16, now the total mean-input current can be expressed as

$$\langle I^{a\theta,\mathrm{tot}} \rangle = \sqrt{K_0}\hat{I}_a^{\mathrm{ext}}(1 + \epsilon\cos 2(\theta - \theta_0)) \tag{21}$$

$$+ \sum_{b=1}^{2} \sqrt{K_b}\mathfrak{J}_{ab}[r_{b,2} f_0(\theta_c) + \gamma r_{b,2} f_2(\theta_c)\cos 2(\theta - \theta_0)], \tag{22}$$

where

$$f_0(\theta_c) = \int_{-\theta_c}^{\theta_c} \frac{\mathrm{d}\theta'}{\pi}(\cos 2\theta' - \cos 2\theta_c) = \frac{1}{\pi}(\sin 2\theta_c - 2\theta_c \cos 2\theta_c) \tag{23}$$

$$f_2(\theta_c) = \int_{-\theta_c}^{\theta_c} \frac{\mathrm{d}\theta'}{\pi}\cos 2\theta'(\cos 2\theta' - \cos 2\theta_c) = \frac{1}{\pi}\left(\theta_c - \frac{1}{4}\sin 4\theta_c\right). \tag{24}$$

(We have borrowed the notation from Ben-Yishai et al. (1995) who studied a different kind of model that contains similar expressions; see also Hansel and Sompolinsky (1998)). Again, the total current Equation 22 has to vanish for all orientation columns θ, so both the constant and the $\cos 2(\theta - \theta_0)$ terms vanish separately:

$$\hat{I}_a^{\mathrm{ext}} + \sum_{b=1}^{2} \hat{\mathfrak{J}}_{ab} r_{b,2} f_0(\theta_c) = 0 \tag{25}$$

$$\epsilon\hat{I}_a^{\mathrm{ext}} + \gamma \sum_{b=1}^{2} \hat{\mathfrak{J}}_{ab} r_{b,2} f_2(\theta_c) = 0. \tag{26}$$

Dividing Equation 25 by 26 yields

$$\frac{f_2(\theta_c)}{f_0(\theta_c)} = \frac{\epsilon}{\gamma}, \tag{27}$$

which can be solved for θ_c. Note that Equation 27, and thus the tuning width of the mean rates, does not depend on the overall strength of the input, I_a^{ext} (i.e., the 'contrast' of the stimulus). We find therefore contrast-invariant tuning of the mean rates as a result of cortical interactions, in agreement with experimental findings (Sclar & Freeman 1982). Having calculated θ_c, we can find the mean rates with help of Equation 25, via

$$r_{a,2} = -\frac{1}{f_0(\theta_c)} \sum_{b=1}^{2} (\hat{\mathrm{J}}^{-1})_{ab} \hat{I}_b^{\mathrm{ext}}, \tag{28}$$

and by using the equality $r_{a,0} = -r_{a,2} \cos 2\theta_c$.

Input noise spectrum. The preceding calculations show how cortical interactions are responsible for a narrowing of the tuning of the population firing rates, relative to the tuning of the input to the network. We can proceed one step further in our analytical treatment of the mean-field model and consider the tuning of the neuronal input noise spectrum. We can write the dynamic noise in the input current as

$$\left\langle \delta I_{a\theta}^{\mathrm{rec}}(t) \delta I_{a\theta}^{\mathrm{rec}}(t') \right\rangle = \sum_{b=1}^{2} \mathcal{J}_{ab}^2 \int_{-\pi/2}^{\pi/2} \frac{\mathrm{d}\theta'}{\pi} (1 + \gamma \cos 2(\theta - \theta')) C_{b\theta'}(t - t'), \tag{29}$$

where we have used the continuum notation for the weighted averages. The correlation function $C_{b\theta'}(t - t')$ has a piece proportional to $r_b(\theta)\delta(t - t')$, which gives

$$\lim_{\omega \to \infty} \left\langle \left| \delta I_{a\theta}^{\mathrm{rec}}(\omega) \right|^2 \right\rangle = \sum_{b=1}^{2} \mathcal{J}_{ab}^2 \int_{-\pi/2}^{\pi/2} \frac{\mathrm{d}\theta'}{\pi} (1 + \gamma \cos 2(\theta - \theta')) r_{b\theta'} \tag{30}$$

$$= \sum_{b=1}^{2} \mathcal{J}_{ab}^2 [r_{b,2} f_0(\theta_c) + \gamma r_{b,2} f_2(\theta_c) \cos 2(\theta - \theta_0)]. \tag{31}$$

To obtain Equation 31, we performed calculations analogous to the ones for solving the integrals for the rate equations. Using Equations 27 and 28, we can then write the flat contribution to the noise spectrum as

$$\lim_{\omega \to \infty} \left\langle \left| \delta I_{a\theta}^{\mathrm{rec}}(\omega) \right|^2 \right\rangle = -\hat{I}_a^{\mathrm{ext}} [1 + \epsilon \cos 2(\theta - \theta_0)] \sum_{b=1}^{2} \mathcal{J}_{ab}^2 \sum_{c=1}^{2} (\hat{\mathbf{J}}^{-1})_{bc} \hat{I}_c^{\mathrm{ext}}. \tag{32}$$

This result states that the high-frequency limit of the neuronal input noise has the same orientation tuning as the external input to the neuron.

For $t \neq t'$, it is not possible to calculate analytically solutions to Equation 29 because the correlation function $C_{b\theta'}(t - t')$ needs to be evaluated numerically. Similarly, the tuning of the irregularity in the neuronal firing (as described by, e.g., the Fano factor) can only be determined by solving the full mean-field model numerically.

Numerical procedure

We use an iterative approach that was originally developed for spin glass models (Eisfeller & Opper 1992) to find self-consistent solutions of the firing statistics given by the rates $r_{a\theta}$, the rate fluctuations $\overline{(r_j^{a\theta})^2}$, and the correlations $C_{a\theta}(t - t')$ (see Equations 9–13). We start with initial estimates of these quantities, which we obtain by using a white-noise approximation and the analytical treatment described above. We then generate many realizations of Gaussian synaptic currents using Equations 4 and 9, which we use to drive single integrate-and-fire neurons. By collecting their firing statistics, we obtain improved estimates of the rates, rate fluctuations and correlations. These are then used to repeat the cycle until the input and output statistics are consistent. What follows is a more detailed description of how we implemented this general approach for the orientation hypercolumn model.

In our calculations, we modeled the hypercolumn as an assembly of 30 orientation columns, with their preferred orientations θ equally spaced between $-\pi/2$ and $\pi/2$ (or between -90 and 90 degrees, as in the figure captions). We used parameter values corresponding to expected numbers of $K_1 = 4000$ excitatory inputs and $K_2 = 1000$ inhibitory

inputs to each neuron. For simplicity, we chose a membrane time constant of $\tau = 10$ ms for all neurons. The generic intra-cortical connection strengths $\mathcal{J}_{ab}$ in (2) were taken as

$$\begin{pmatrix} \mathcal{J}_{11} & \mathcal{J}_{12} \\ \mathcal{J}_{21} & \mathcal{J}_{22} \end{pmatrix} = \begin{pmatrix} 0.5 & -2 \\ 1 & -2 \end{pmatrix}. \tag{33}$$

The synaptic strengths of the afferent inputs from the LGN were taken to be stronger for the excitatory neurons; specifically, in Equation 4, we chose $I_2^{\text{ext}} = \frac{2}{3} I_1^{\text{ext}}$. To study the role of the overall strength of synapses, we multiplied the generic synaptic weights (including the strength of the external input) by a common scaling factor $\mathcal{J}_s$.

To solve the mean-field equations for a specific set of network parameters, we proceed in two steps. First, we calculate the average firing statistics for all sub-populations $a\theta$, $a \in \{1, 2\}$, $\theta \in \{1, \ldots, 30\}$. Then, we calculate the necessary statistics for investigating single-neuron properties.

The first step requires obtaining the average firing statistics of all sub-populations $a\theta$ at all stimulus orientations θ_0 and all stimulus contrasts I_a^{ext} of interest. However, at this stage, we only need to probe the network at one stimulus orientation (but at all contrasts) because of the inherent symmetry in the network topology. A shift in stimulus orientation θ_0 corresponds to a shift in the labeling of the orientation columns of equal magnitude and opposite direction. In addition, we only need to run simulations for half of the columns θ and mirror the results for the other half.

To collect the average firing statistics from a sub-population $a\theta$, we simulate many trials of single neurons that are sampled from within that sub-population. This is achieved by generating Gaussian input currents according to the mean-field description given by Equation 9. For the first iteration, we use the approximate mean rates $r_{b\theta'}$ derived from our analytical treatment (Equation 28), white noise approximations for the correlations (i.e., $r_{b\theta'}\delta(t - t')$ instead of $C_{b\theta'}(t - t')$), and $r_{b\theta'}^2$ in place of $\overline{(r_j^{b\theta'})^2}$. We effectively sample different neurons in the sub-population $a\theta$ by drawing a different set of random numbers $x_{b\theta'}$ for each trial. We thus obtain a large number of spike trains that provide us with new 'output' firing statistics for this specific sub-population $a\theta$ when driven with 'input' statistics of all sub-populations $b\theta'$. Within the first iteration, this step is repeated for different choices of a and θ until we have obtained output statistics for all sub-populations $a\theta$. For the next iteration, we update all input statistics using a small step size of order $1/\sqrt{K_0}$ towards the output statistics, followed by again collecting new output statistics via simulating many single neurons. As already mentioned, these steps are repeated until input and output statistics agree. How do we estimate the average rates, rate fluctuations and correlations from the spike trains? The average rates are simply obtained via the average spike counts; the correlations from calculating the $T \times T$ covariance matrix of the spike matrix, where T is the trial length in time steps; and we estimate the average rate fluctuations from the long-tail offset of the spike autocorrelation function, which stems from the trial-to-trial rate variations of the different neurons. Specifically, we have for $|t - t'| \to \infty$:

$$C_{b\theta'}(t - t') \to \overline{\left(r_j^{b\theta'} - r_{b\theta'}\right)^2} = \overline{\left(\delta r_j^{b\theta'}\right)^2}. \tag{34}$$

Once this first part of the procedure converges, which usually takes tens of iterations, one has obtained a set of self-consistent average firing statistics, describing the population responses for a specific stimulus contrast. Equipped with these population statistics we can then proceed to the second part to obtain the necessary information for calculating input statistics and firing statistics for individual neurons.

To collect statistics from a single neuron rather than from a population of neurons, we need to examine the description of the 'static part of the noise' in the input current (Equation 11), reflected by the Gaussian random numbers $x_{b\theta'}$, more closely. These random numbers reflect the fact that the overall strength of the input current from the presynaptic sub-population $b\theta'$ varies randomly from neuron to neuron for a given stimulus. That random offset of the mean of the Gaussian input current has two sources: first, there is intrinsic variability in the connectivity, i.e., the number of inputs from presynaptic population $b\theta'$ varies from one neuron to the next. This contribution to the offset is stimulus-independent and neuron-specific. Second, there is intrinsic variability in the presynaptic firing rates because the fraction of presynaptic neurons that actually contributes to the input of a single neuron constitutes a random sample drawn from a population of neurons with a distribution of rates. The distribution of rates, and thus the contribution to the offset from this source, is potentially stimulus-dependent. We can separate these two contributions formally by writing

$$\left(\overline{\left(r_j^{b\theta'}\right)^2}\right)^{\frac{1}{2}} x_{b\theta'} = r_{b\theta'} y_{b\theta'} + \left(\overline{\left(\delta r_j^{b\theta'}\right)^2}\right)^{\frac{1}{2}} z_{b\theta'}, \tag{35}$$

where $y_{b\theta'}$ and $z_{b\theta'}$ are independently drawn from a unit-variance normal distribution, reflecting the variability in connectivity and the variability in presynaptic firing rates, respectively. Before we can collect statistics from a single neuron (defined by a set of connectivity factors $y_{b\theta'}$) under various stimulus conditions, we need to determine how strong the $z_{b\theta'}$-values can fluctuate from one specific stimulus to another one. In other words, we need to know the amount of correlations between the $z_{b\theta'}$-values for all stimuli under consideration. This correlation structure can be determined self-consistently, with an iterative approach analogous to the procedure for calculating the temporal correlations in the spike trains: Starting with an initial guess for the correlation structure between the rate variations $\overline{(\delta r_j^{b\theta'})^2}$ under all stimulus conditions, we generate correlated $z_{b\theta'}$-values for many single neurons for all of these stimuli. We then simulate these neurons under all conditions and collect statistics of the resulting rate fluctuations and their correlations. These correlations are then used in the next iteration for generating new sets of correlated $z_{b\theta'}$-values, followed by simulations and data collection. The steps are repeated until the input and output-correlation structures agree. This algorithm converges within a few steps (less than 10 in all our simulations) in its naive form, where the output statistics of the previous iteration are directly used as the input statistics for next one. Moreover, we found the algorithm to be robust with respect to the initial guess. Both extremes, starting from perfect correlations (identical $z_{b\theta'}$-values for all stimuli) and from no correlations (independently drawn $z_{b\theta'}$-values for each stimulus), resulted in convergence to the same structures within a few steps.

Results

We concentrate first on results describing response characteristics of neurons obtained from their firing statistics. These results can be compared directly with known properties of orientation selective neurons in V1 like contrast-invariant tuning or the variability in spike counts for repeated presentations of the same stimulus. We then describe results pertaining to properties of the neuronal input currents (and their orientation tunings) for the present hypercolumn model.

Tuning of the neuronal firing

A prominent feature of orientation selective neurons in primary visual cortex is an invariance of the tuning width with respect to stimulus contrast. From our approximate analytical

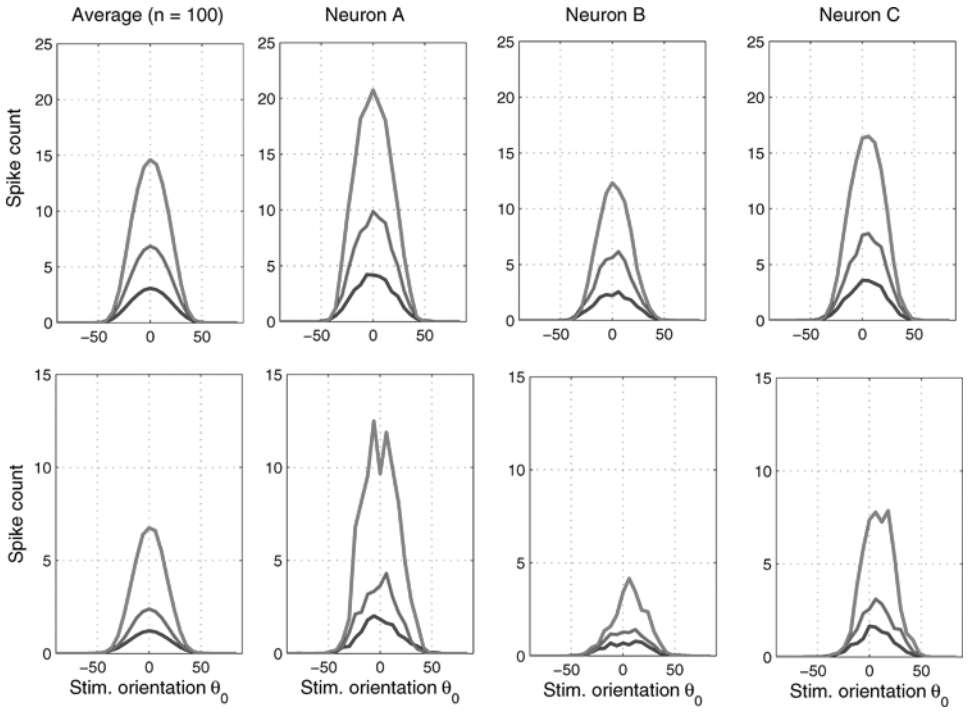

Figure 2. Orientation tuning of the firing rates. Firing rates as a function of stimulus orientation at three different contrasts $\hat{I}_a^{\text{ext}} = 0.5$, 1, and 2 (lower, middle, and upper curve in each panel) for randomly chosen single neurons, denoted *A*, *B* and *C*, and for an average over 100 neurons (left panels). The tuning width is invariant with respect to contrast for both the average tuning curves and single neuron tuning curves, despite the higher irregularity in the shapes for single neurons. Stronger synaptic connections in the network result in more irregular tuning curves for single neurons: *Upper row:* Moderately strong synapses ($\mathcal{J}_s = 0.7$). *Lower row:* Strong synapses ($\mathcal{J}_s = 1.2$).

treatment of the present model, we expect such a contrast invariance on average over neurons within an orientation column (see Equation 27). Our numerical results confirm this prediction. Figure 2 shows examples of tuning curves collected from neurons with preferred orientation $\theta = 0$ at three different contrasts $\hat{I}_a^{\text{ext}} = 0.5$, 1, and 2 (the lower, middle, and upper curve within each panel, respectively) and two different overall synaptic strengths ($\mathcal{J}_s = 0.7$ and 1.2; upper row and lower row, respectively). The parameter values for the feedforward tuning from the LGN and for the tuning of the intra-cortical connectivity were $\epsilon = 0.5$ and $\gamma = 0.625$, respectively, resulting in a predicted tuning width of 43.2 degrees, according to the analytical approximation (Equation 27). The average tuning curves over 100 single neurons (left-most panels in Figure 2) are smooth and exhibit contrast-invariance. The shapes of the tuning curves are well described by threshold-cosine functions, as predicted by our analytical approximation, except for low rates close to the critical angle θ_c, where we observe a rounded fall-off to zero with non-zero rates for angles just outside the analytically predicted tuning width. Similarly, we observe an almost linear dependence of the firing rate on the stimulus contrast (see Equation 28) except for low rates. In the upper row of Figure 2, doubling the contrast results in approximately doubling the firing rate, while in the lower row of Figure 2, where in this example the overall rates are low even at the preferred orientation, the relationship is not exactly linear. (Note the different scalings of the y-axes in the upper versus the lower panels.) Spike counts in our figures belong to trials of 100 ms duration.

Figure 2 also shows examples of single-neuron tuning curves, providing a more direct comparison of the model with experimental data. While the average tuning is both smooth and symmetric, the tuning curves of single neurons show some distortions and asymmetries. Part of this irregularity stems from the inherent variability in connectivity. The connectivity pattern for a specific neuron is defined by a set of 60 random numbers $y_{b\theta'}$: $b \in \{1, 2\}$, $\theta' \in \{1, \ldots, 30\}$, which underlies the idiosyncratic overall shapes, magnitudes, and asymmetries seen in the tuning curves of the three neurons *A*, *B*, and *C* in Figure 2. However, the increased overall irregularity for stronger synapses ($\mathcal{J}_s = 1.2$ in the lower panel of Figure 2 as compared to $\mathcal{J}_s = 0.7$ in the upper panel) is a signature of another contribution: the inherent variability in the firing rates. The latter depends on – and increases with – the overall strength of the synapses, as we will show below in more detail. It can also be seen in Figure 2, that, despite the somewhat irregular shapes, the contrast-invariance of the tuning width is a property not only of the average firing rate in our model, but also of individual neurons.

We characterize the irregularity in the neuronal firing by the Fano factor F. For a Poisson process $F = 1$, while $F \neq 1$ implies temporal correlations in the spike times: $F > 1$ indicates a tendency towards 'bursty' spiking behavior, and $F < 1$ indicates more regular spike trains with narrower interspike interval (ISI) distributions. Figure 3 shows the tuning of the Fano factor for three different overall connection strengths $\mathcal{J}_s = 0.4$, 0.7, and 1.2. As in Figure 2, the results for (the same) three individual neurons are shown, as well as an averaged tuning curve. It can be seen that the Fano factor depends systematically on the overall strength of connectivity: stronger synapses lead to more irregular spike counts.

The averaged tuning curves possess a further characteristic that we observed consistently in our simulations performed with various sets of parameters: if Fano factors are considerably higher (lower) than 1 at the preferred orientation, then they are so for all stimulus orientations. In addition, the Fano factors are then maximal (minimal) at the PO, declining (rising) closer to 1 as the difference between the stimulus orientation and the preferred orientation increases.

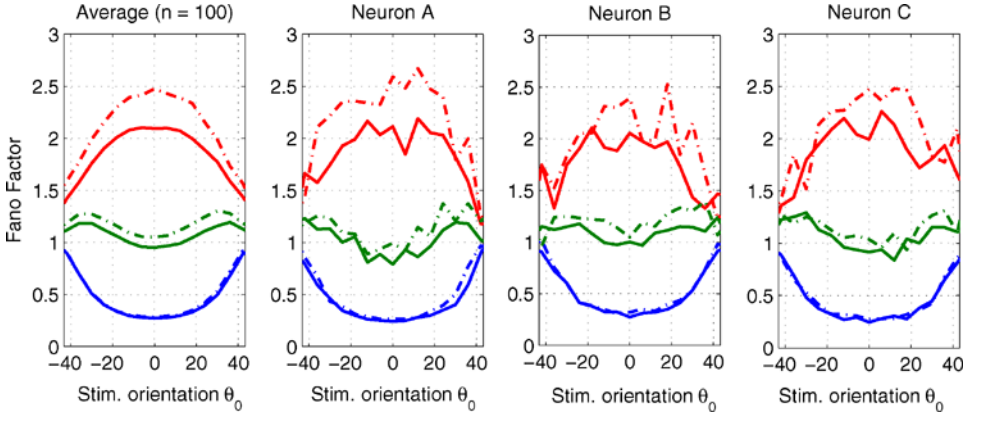

Figure 3. Tuning of the Fano factors. Neurons *A*, *B* and *C* are the same as in Figure 2. Fano factors depend sensitively on the overall synaptic strength, scaled by the parameter $\mathcal{J}_s$. Weak synapses ($\mathcal{J}_s = 0.5$, blue) result in Fano factors below 1, moderately strong synapses ($\mathcal{J}_s = 0.7$, green) result in approximate Poisson statistics, i.e., $F \approx 1$, while strong synapses result in Fano factors exceeding 1 ($\mathcal{J}_s = 1.2$, red). The Fano factor-sensitivity on synaptic strength is strongest at the preferred orientation, while stimuli close to the tuning width elicit firing statistics closer to Poisson. Also shown in this figure is a comparison between instantaneous synaptic dynamics (solid lines) and synaptic filtering with a time constant of $\tau_s = 4$ ms (dash–dot lines). Synaptic filtering causes somewhat higher Fano factors, which is more pronounced for stronger synapses, but the qualitative behavior is already captured by instantaneous synapses in this model.

However, this property does not hold exactly when Fano factors are close to 1, as the curves in Figure 2 for $\mathcal{J}_s = 0.7$ show. Nevertheless, if the Fano factor is close to 1 at the PO, then its tuning curve is nearly flat.

For simplicity, we formulated our model with instantaneous synaptic currents, rather than including synaptic dynamics with more realistic temporal shapes of the postsynaptic currents. We tested, however, whether such a simplification is justified for our model or whether this approach obscures important parts of the dynamics that might control the amount of irregularity in the spike trains. It is straightforward to account for synaptic dynamics in the mean-field formulation by replacing the correlation function of the spike trains (Equation 13) with the correlation function of the synaptically filtered spike trains. Our approach of explicitly simulating neuronal and synaptic dynamics for solving the the mean-field equations numerically makes it especially simple to generalize the model in this direction. We tested our model with synaptic filter kernels $K(t)$ of the form

$$K(t) = \frac{1}{\tau_2 - \tau_1} \left(\mathrm{e}^{-t/\tau_2} - \mathrm{e}^{-t/\tau_1} \right) \tag{36}$$

for various values of synaptic time constants τ_1 and τ_2, but observed only a weak dependence of the firing characteristics on time constants up to 16 ms. We show an example in Figure 3, where we overlayed simulation results for $\tau_1 = 0$ and $\tau_2 = \tau_s = 4$ ms (dash-dot lines), corresponding to a postsynaptic current that decays exponentially with a time constant of 4 ms. Synaptic filtering increases the tendency of 'burstiness' (positive temporal correlation between spikes for short time lags), provided that such burstiness is present even without synaptic filtering. Thus, synaptic filtering increases Fano factors bigger than 1 as compared to instantaneous dynamics, but the increases were moderate in all cases we investigated and did not change the general qualitative temporal firing characteristics in the present model.

As already mentioned, Fano factors that deviate from 1 indicate temporal correlations in the spike trains. The nature of these correlations and their orientation dependence is summarized in Figure 4 for a case with $F < 1$ ($\mathcal{J}_s = 0.5$; upper panels) and a case with $F > 1$ ($\mathcal{J}_s = 1.3$; lower panels) for both excitatory neurons (left panels) and inhibitory ones (right panels). For $\mathcal{J}_s = 0.5$, there is a negative dip for small time differences, indicating a relative refractoriness to emitting a spike immediately after a previous one. For stronger synapses ($\mathcal{J}_s = 1.3$) there is no such refractoriness. On the contrary, for strong synapses, we observe positive correlations for small time differences. For both strong and weak synapses, the correlations are strongest at the preferred orientation and decrease monotonically for less optimal stimulus orientations. The autocorrelations for excitatory and inhibitory neurons show the same qualitative features, differing only in their overall size.

In Figure 5, we illustrate how the firing statistics depend on ϵ and γ, which determine how strongly the input current and the intracortical connectivity are tuned (see Equations 4 and 1, respectively). Fano factor tuning curves (left panels) and firing rate tuning curves (right panels) for three different combinations of ϵ and γ are shown, parameterized by $\mathcal{J}_s$, the scaling factor for the synaptic strengths.

As shown analytically above, the ratio ϵ/γ determines the tuning width of the neuronal firing (see Equation 27). This is reflected by the identical firing tuning widths in the first and second row of Figure 5, for both of which $\epsilon/\gamma = 0.8$, resulting in a tuning width of $\theta_c = 43.2$ degrees. The third row of Figure 5 shows results for the same external input tuning $\epsilon = 0.5$ as in the first row, but for a different ratio $\epsilon/\gamma = 0.6$. This results in $\theta_c = 67.7$ degrees and an accordingly broader tuning curve of the firing, plotted in the right panel of the third row. The curves for the Fano factor tuning in the left panels of Figure 5 suggest that the tuning of

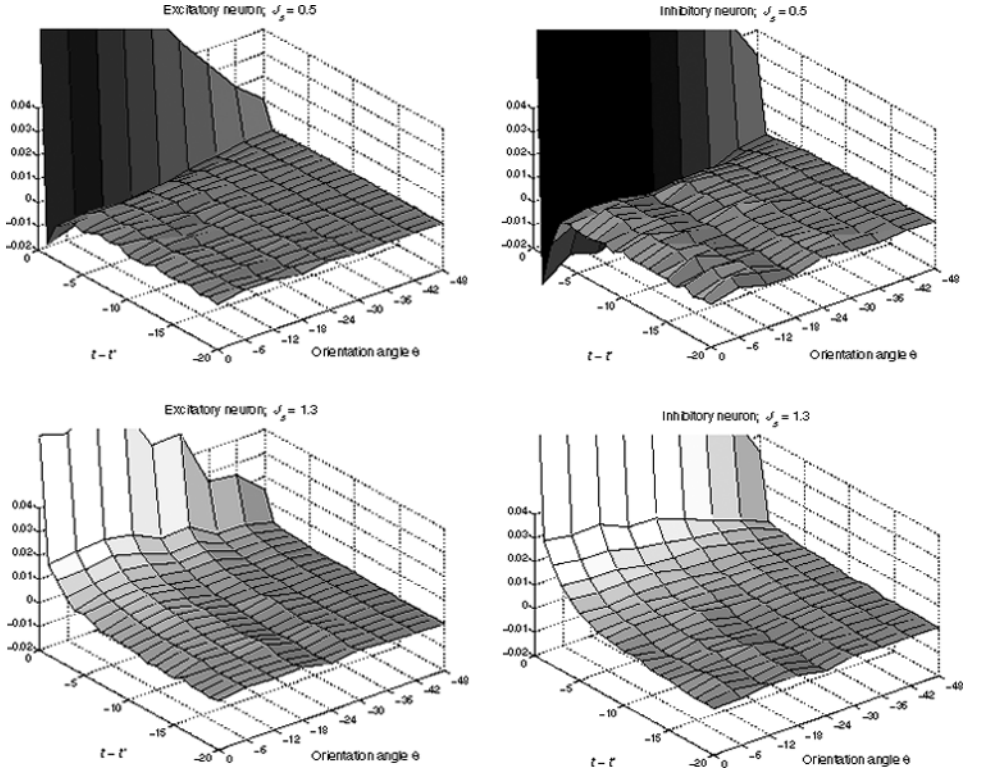

Figure 4. Autocorrelation tuning. *Upper panels:* Weak synapses with $\mathcal{J}_s = 0.5$. There is a dip to negative values for small time differences. It decreases in strength at greater time differences. The dip indicates a relative refractoriness to emitting a spike immediately after a previous one, resulting in Fano factors $F < 1$. *Lower panels:* Strong synapses with $\mathcal{J}_s = 1.3$. There is a hill of positive correlations for short intervals, falling off to zero for increasing time differences. The hill indicates a tendency toward clustered spikes, resulting in $F > 1$. The autocorrelations for excitatory neurons (left panels) and inhibitory neurons (right panels) show the same qualitative features, differing only in overall size.

the firing irregularity is – just as the tuning of the firing itself – only dependent on the ratio ϵ/γ. (We consistently found this dependence in all our simulations.)

Tuning of the neuronal input current

Our analytical treatment of the balanced hypercolumn model reveals that the high-frequency neuronal input noise power has the same tuning as the external input. In Figure 6, we show simulation results of the noise tuning for the same three combinations of ϵ and γ as in Figure 5. For the panels in the first and the second row of Figure 6, $\epsilon/\gamma = 0.8$, but $\epsilon = 0.5$ and $\epsilon = 0.25$ in the upper and middle rows, respectively. While the tuning of the neuronal firing is identical for these two cases, the noise tuning is weaker in the middle row, reflecting the weaker tuning of the external input (left panels). The results presented in the third row of Figure 6 show a case with a broader tuning of the response, resulting from a different ratio between ϵ and γ, but with the same $\epsilon = 0.5$ as in the first row. For these two cases, the tunings on the input side – concerning external input and dynamic noise – are practically indistinguishable, while the tunings of the firing differ. Thus, the noise tuning is determined by ϵ, unlike the response tuning, which depends on the ratio ϵ/γ.

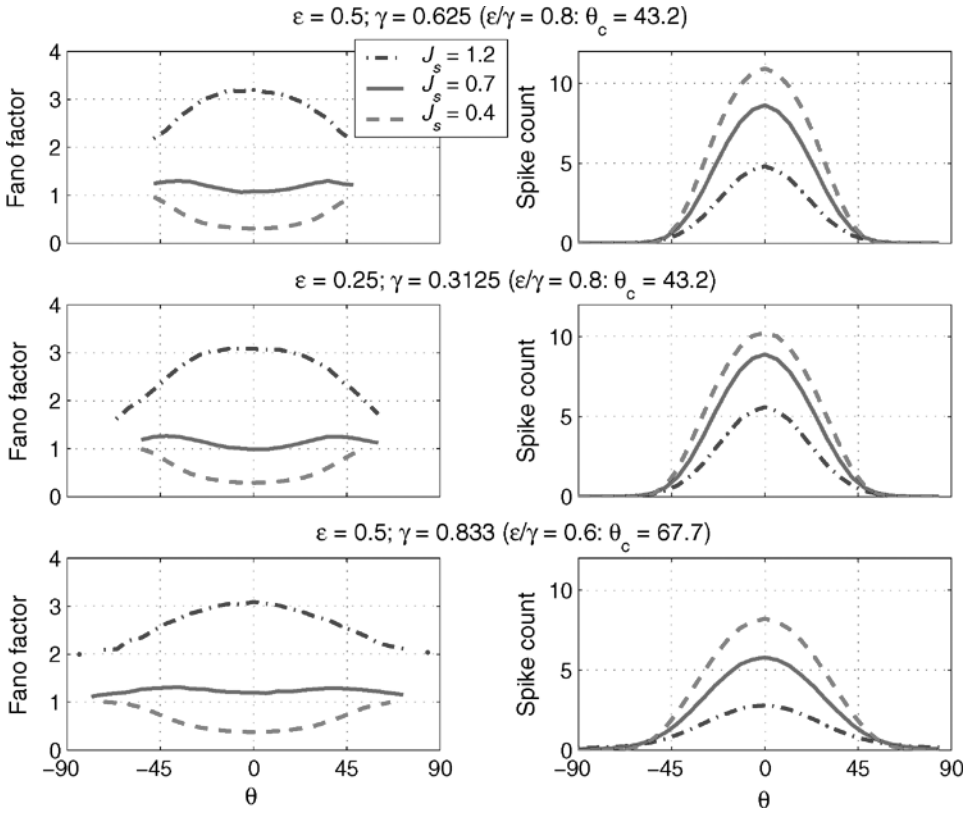

Figure 5. Dependence of the Fano factors on tuning parameters ϵ and γ at three different values of relative synaptic strengths $\mathcal{J}_s$. Fano factors and mean spike counts are shown for three different combinations of ϵ (external input tuning) and γ (connectivity tuning). The tuning of both the Fano factors and the mean counts are controlled by the ratio ϵ/γ.

The balanced state for the orientation hypercolumn implies that the mean input currents (external and recurrent currents), which are each of $\mathcal{O}(\sqrt{K_a})$ with $K_a \gg 1$, cancel up to corrections of $\mathcal{O}(1)$. It is not straightforward to calculate the tuning of the resulting net mean current, since the balance condition (Equation 14) does not allow inferences about its size. However, the solutions obtained by the numerical algorithm provide direct access to the net mean currents, which we depict in Figure 7 for the same combinations of ϵ and γ as for the noise tuning in Figure 6. It is clear from Figure 7 that the tuning of the mean input, unlike the dynamic input noise tuning, is not determined by the tuning of of the external input. Rather, it seems to be the ratio ϵ/γ that primarily determines it, as suggested by the almost identical tunings for the two cases with identical ϵ/γ. Since the tuning of the external input and that of the noise variance are the same, the left panels of Figure 7 also show how the tuning of the noise compares to that of the mean input current for the three combinations of ϵ and γ.

Discussion

In this work, we presented a complete mean field theory for a balanced network with structural inhomogeneity, together with an algorithm that allows one to find the self-consistent

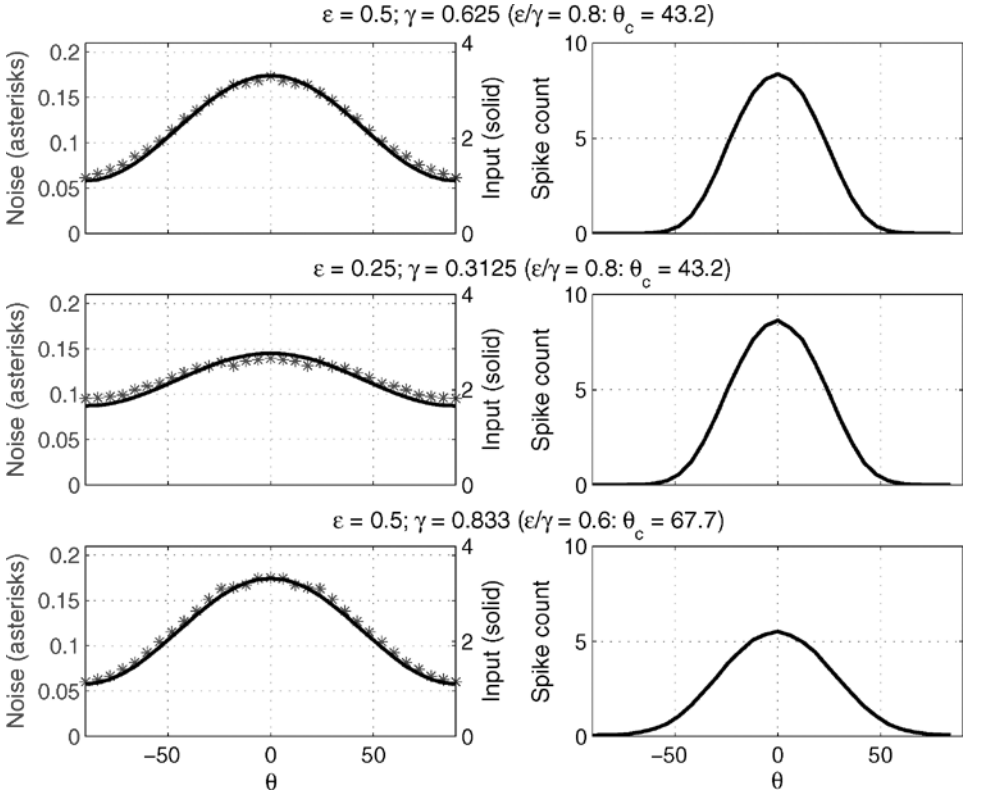

Figure 6. Dependence of the noise on tuning factors ϵ and γ. External input and dynamic input noise versus tuning of the neuronal firing for the same three combinations of ϵ and γ as in Figure 5. It can be seen that the tuning of the noise is determined by ϵ, while the tuning of the firing rate is determined by the ratio ϵ/γ.

solutions for the mean rates, their cell-to-cell fluctuations, and the correlation functions. We applied the theory to a simple model of an orientation hypercolumn in primary visual cortex, comprised of integrate-and-fire neurons. Despite the relative simplicity of the model, the resulting dynamics capture several key properties known about responses of orientation selective cortical neurons *in vivo*. Within this description, we can pinpoint how the resulting neuronal dynamics are controlled by parameters of the model, and quantify their influence.

Specifically, we find contrast-invariant tuning of the neuronal firing not only for the population rates, as derived from the analytical treatment, but also for single, randomly chosen neurons. Moreover, the firing rate increases linearly with the strength of the input current (i.e., the contrast of the stimulus). Note that these are network effects originating in the dynamical balance between excitation and inhibition, not properties of isolated neurons. This is in agreement with experimental results, where such a linear input–output relationship can only be found for cortical neurons *in vivo*, but not for single neurons *in vitro*.

Another network effect that emerges naturally from the self-consistent dynamic balance, in combination with the static randomness in the connectivity, is the irregularity in the neuronal firing. We are able to describe it quantitatively through the correlation functions, which are determined self-consistently in the theory. Such firing-statistical issues cannot be addressed in 'rate models', which simply assume a particular relation between average input current or membrane potential and firing rate. While it is possible to calculate the firing variability

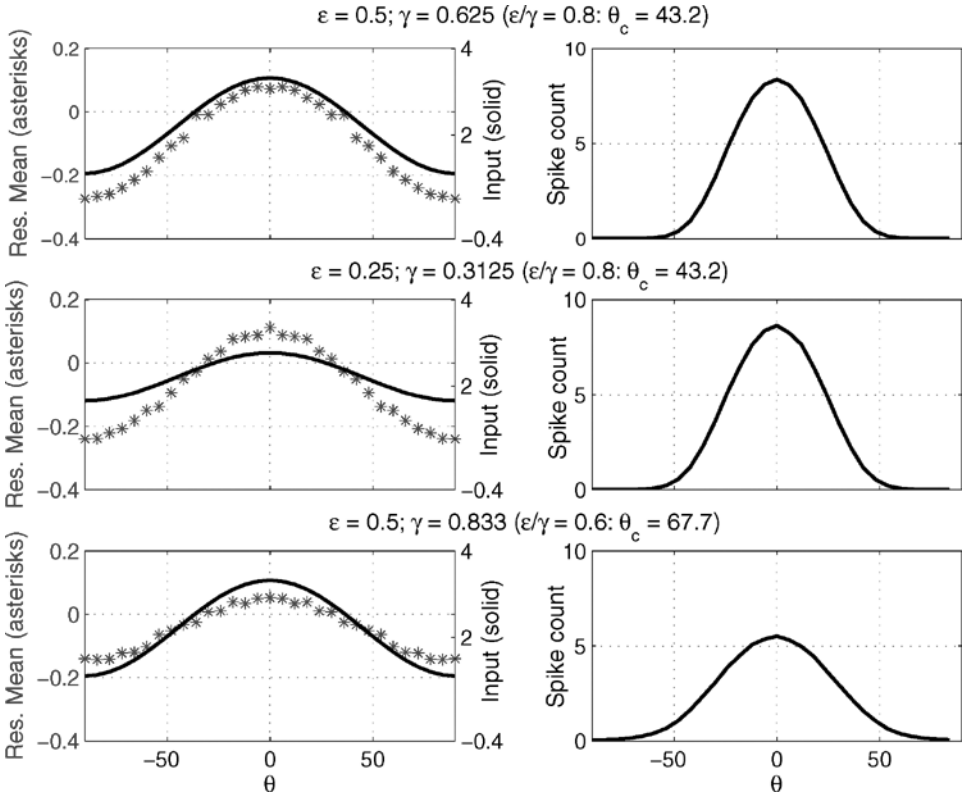

Figure 7. Dependence of the mean input current on tuning factors ϵ and γ. External input tuning and mean-input tuning versus tuning of the response for the same three combinations of ϵ and γ as in Figures 5 and 6. The tuning of the mean input is not determined by ϵ; rather, as for the spike count tuning shown in the right panels, the ratio ϵ/γ plays an important role.

in the mean-field treatment of (Brunel 2000), it cannot be done in a self-consistent manner because of the assumption that the neuronal input is uncorrelated in time (white noise). Here, we color the noise self-consistently. Poisson-like statistics (Fano factor $F = 1$) are only one possibility within a continuum of firing statistics that depend sensitively on the strengths of the synapses: stronger synapses generally lead to higher Fano factors. The underlying mechanism can be summarized as follows: Stronger synapses increase the probability of a spike shortly after reset, which leads to a higher tendency of spikes occurring in 'clusters', thereby increasing the spike count variance. A detailed account of this mechanism, involving the dependence of the membrane potential distribution on the synaptic strength can be found in (Lerchner et al. 2006), where the analysis was carried out for a single cortical column.

We have concentrated on instantaneous synaptic currents in the present model because the dependence of firing irregularity on synaptic filtering is weak, as shown in Figure 3. The situation becomes quite different if conductance-based synapses are considered rather than current-based ones, where the emergence of high-conductance states makes the neuronal dynamics very sensitive to even short synaptic time constants, as discussed in (Lerchner et al. 2004).

The mean field theory applied to the present model allows us to study tuning properties of both the neuronal firing and the neuronal input and their dependence on network parameters.

Concerning the irregularity of firing, our results suggest that the Fano factor F tend to stay either well above 1, right around 1, or well below 1 for all orientations. That is, one never finds a neuron with strongly super-Poissonian firing at one stimulus orientation and strongly sub-poissonian firing at another. This appears to be true for individual neurons as well as for population averages. Moreover, the modulation strength of F over angles increases, relative to the almost untuned case of $F \approx 1$, with increasing (resp. decreasing) overall values of F, reaching a maximum (resp. a minimum) at the preferred orientation.

Concerning the tuning of the input currents, we find analytically that the high-frequency input noise power has the same tuning as the external input to the neuron (which in turn is determined by a Hubel–Wiesel feed-forward connectivity from the LGN). In our numerical calculations, we observe a close fit between the tuning of the overall input noise and the one of the external input. This suggests that the tuning of the external input may be a good predictor for the noise tuning, and vice versa. In contrast, we find that the tuning of the mean input current does not reflect the one of the external input, but is predominantly determined by the ratio ϵ/γ of the modulation strengths of the external input and the cortical interactions.

Anderson et al. (2000) demonstrated how the right amount of irregularity ('noise') in the membrane potentials of cortical neurons can contribute to a contrast-invariant tuning width, provided that the membrane potential is in itself contrast-invariant and that there is a threshold-linear relationship between (noiseless) firing rate and membrane potential. In the present work, none of these important properties need to enter the model as assumptions. On the contrary, they emerge as consequences from the model and are all explained within this single framework, as discussed above.

Some of our results (the existence of a stable, asynchronous low-rate state, contrast-invariant orientation tuning, and the inverse relation between the sharpness of orientation tuning and intracortical tuning strength γ) were obtained previously by Wolf et al. (2001) in an extension of van Vreeswijk and Sompolinsky's stochastic binary model (van Vreeswijk & Sompolinsky 1996, 1998) to a hypercolumn, but the treatment of a spiking neuron model and all the results for correlations of both input and output are new here. Also new is that we go beyond population statistics and make quantitative predictions about input and output characteristics of *individual* neurons, which can be tested directly.

Firing irregularity of neurons in primary visual cortex has been investigated experimentally for a long time (see, e.g., Heggelund & Albus 1978; Dean 1981; Tolhurst et al. 1981; Snowden et al. 1992; Gershon et al. 1998). Well studied is also the dependence of firing rate on the stimulus orientation (Sclar & Freeman 1982; Skottun et al. 1987), but we are not aware of studies investigating the dependence of firing irregularity on the orientation. Our predictions concerning the tuning of the input currents (for both mean and noise) can be tested experimentally by systematically changing ϵ (the external input tuning strength) via changing the spatial modulation of the stimulus and then observing how the the mean and noise tunings are affected separately.

The mean field theory presented here, in combination with the numerical procedure for finding the self-consistent solutions, can be applied to models that capture more of the known neuronal and cortical physiology. For example, it is straightforward to incorporate conductance-based synapses into the hypercolumn model, as has already been done for a single-column model (see Hertz et al. 2004; Lerchner et al. 2006). It is also straightforward to use different, possibly more realistic neuron models – even several kinds of neuron models within one given network model, since the neuronal dynamics are explicitly simulated within the numerical procedure for collecting the firing statistics. Here, we have shown how the theory can be applied to networks with non-homogenous architecture, using a simple one-dimensional model for a cortical hypercolumn. This model can be thought of as describing

an annulus around a pinwheel center. Using the same general techniques as introduced here, the model can be extended to incorporate a two-dimensional geometry to describe an entire pinwheel. Similarly, as we have shown for orientation selectivity, it is possible to include other coding features, such as spatial phase, for example. Thus, the power of this mean-field approach lies in its generality, which makes it possible to quantify dynamics of balanced, highly connected networks.

Acknowledgements

We would like to thank an anonymous referee who discovered a flaw in the selfconsistent treatment of fluctuation correlations in a previous version of this paper and suggested the procedure to correct it, as described at the end of the section 'Numerical procedure.'

References

Amit D, Brunel N. 1997a. Dynamics of a recurrent network of spiking neurons before and following learning. Network (8):373–404.

Amit D, Brunel N. 1997b. Model of spontaneous activity and local structured activity during delay periods in the cerebral cortex. Cereb Cortex (7):237–252.

Anderson JS, Lampl I, Gillespie DC, Ferster D. 2000. The contribution of noise to contrast invariance of orientation tuning in cat visual cortex. Science (290):1968–1972.

Ben-Yishai R, LevBar-Or R, Sompolinsky H. 1995. Theory of orientation tuning in visual cortex. Proc Natl Acad Sci (USA) (92):3844–3848.

Brunel N. 2000. Dynamics of sparsely connected networks of excitatory and inhibitory spiking neurons. J Comput Neurosci (8):183–208.

Dean AF. 1981. The variability of discharge of simple cells in the cat striate cortex. Exp Brain Res (44):437–440.

Eisfeller H, Opper M. 1992. New method for studying the dynamics of disordered spin systems without finite-size effects. Phys Rev Lett (68):2094–2097.

Fulvi Mari C. 2000. Random networks of spiking neurons: instability in the xenopus tadpole moto-neuron pattern. Phys Rev Lett (85):210–213.

Gershon E, Wiener MC, Latham PE, Richmond BJ. 1998. Coding strategies in monkey v1 and inferior temporal cortex. J Neurophysiol (79):1135–1144.

Hansel D, Sompolinsky H. 1998. Methods in Neuronal Modeling: from Synapse to Networks, chapter Modeling feature selectivity in local cortical circuits. MIT Press, Cambridge, MA, USA.

Heggelund P, Albus K. 1978. Response variability and orientation discrimination of single cells in in striate cortex of cat. Exp Brain Res (32):197–211.

Hertz J, Lerchner A, Ahmadi M. 2004. Mean field methods for cortical network dynamics. Lect Notes in Comp Sci (3146):71–89.

Hertz J, Richmond B, Nilsen K. 2003. Anomalous response variability in a balanced cortical network model. Neurocomputing (52–54):787–792.

Hubel DH, Wiesel DN. 1962. Receptive fields, binocular interaction and functional architecture in the cat's visual cortex. J Physiol Lond (160):106–154.

Kree R, Zippelius A. 1987. Continuous-time dynamics of asymmetrically diluted neural networks. Phys Rev A (36):4421–4427.

Lerchner A, Ahmadi M, Hertz J. 2004. High conductance states in a mean field cortical network model. Neurocomputing (58–60):935–940.

Lerchner A, Ursta C, Hertz J, Ahmadi M, Enemark S. 2006. Response variability in balanced cortical networks. Neural Computation (18):634–659.

Sclar G, Freeman R. 1982. Orientation selectivity in cat's striate cortex is invariant with stimulus contrast. Exp Brain Res (46):457–461.

Skottun B, Bradley A, Sclar G, Ohzawa I, Freeman R. 1987. The effects of contrast on visual orientation and spatial frequency discrimination: a comparison of single cells and behavior. J Neurophysiol (57):773–786.

Snowden RJ, Treue S, Andersen RA. 1992. The response of neurons in areas v1 and mt of the alert rhesus monkey to moving random dot patterns. Exp Brain Res (88):389–400.

Softky WR, Koch C. 1993. The highly irregular firing of cortical cells is inconsistent with temporal integration of random EPSPs. J Neurosci (13):334–350.

Sompolinsky H, Shapley R. 1997. New perspectives on the mechanisms for orientation selectivity. Curr Opinion Neurobiol (7):514–522.

Tolhurst DJ, Movshon JA, Thompson ID. 1981. The dependence of response amplitude and variance of cat visual cortical neurones on stimulus contrast. Exp Brain Res (41):414–419.

van Vreeswijk C, Sompolinsky H. 1996. Chaos in neuronal networks with balanced excitatory and inhibitory activity. Science (274):1724–1726.

van Vreeswijk C, Sompolinsky H. 1998. Chaotic balanced state in a model of cortical circuits. Neural Comp (10):1321–1371.

Wolf F, van Vreeswijk C, Sompolinsky H. 2001. Chaotic activity induces contrast invariant orienation tuning. In: Soc Neurosci Abstr, volume 12.7.